Liquid Crystals
Publication details, including instructions for authors and subscription information:
http://www.informaworld.com/smpp/title~content=t713926090

New AFLC: a trimesogen presenting antiferroelectric smectic C phase (SmCA) and twist grain boundary smectic A phase (TGBA)

Min-Hui Li; Laurent Detre; Philippe Cluzeau; Noel Isaert; Huu-Tinh Nguyen

Online publication date: 06 August 2010

To cite this Article Li, Min-Hui , Detre, Laurent , Cluzeau, Philippe , Isaert, Noel and Nguyen, Huu-Tinh(1998) 'New AFLC: a trimesogen presenting antiferroelectric smectic C phase (SmCA) and twist grain boundary smectic A phase (TGBA)', Liquid Crystals, 24: 3, 347 — 359
To link to this Article: DOI: 10.1080/026782998207154
URL: http://dx.doi.org/10.1080/026782998207154

LIQUID CRYSTALS, 1998, VOL. 24, NO. 3, 347–359

New AFLC: a trimesogen presenting antiferroelectric smectic C* phase (SmC_A^*) and twist grain boundary smectic A phase (TGBA)

by MIN-HUI LI*, LAURENT DETRE†, PHILIPPE CLUZEAU†, NOEL ISAERT† and HUU-TINH NGUYEN

Centre de Recherche Paul Pascal, CNRS, Avenue Docteur A. Schweitzer, 33600 Pessac, France

†Laboratoire de Dynamique et Structure des Matériaux Moléculaires, CNRS/Université de Lille I, U.F.R. de Physique, 59655 Villeneuve d'Ascq Cedex, France

(*Received 18 July 1997; accepted 22 September 1997*)

A first oligomeric antiferroelectric liquid crystal, a cyclohexane based trimesogen, was synthesized. It was characterized by microscopic observation, differential scanning calorimetry, helical pitch measurement, X-ray diffraction and electro-optical study. A large domain of antiferroelectric phase ($\Delta T \approx 55°C$) and a very rich polymorphism (SmC_A^*, SmC*, SmC_{FI}^*, SmC*, TGBA, BP) are exhibited by the trimesogen.

1. Introduction

Since the discovery of the antiferroelectric smectic phases [1, 2], their fundamental interest and potential applications have stimulated the search for new antiferroelectric materials [3–12]. The SmC_A^* phase has already been confirmed to exist in more than 300 low molar mass compounds and new molecules continue to be synthesized. Recently, interest in dimeric systems has developed, and Suzuki *et al.* [7] have reported an antiferroelectric symmetric dimesogen where two mesogenic moieties are linked by an aliphatic spacer. Poths *et al.* [8] also reported at the Fifth International Conference on FLCs at Cambridge a symmetric dimesogen linked by a siloxane spacer. Non-symmetric dimesogens have also been synthesized and studied [9]. Chiral side group liquid crystalline polymers [10–12] are also known to exhibit antiferroelectric behaviour. Some examples of antiferroelectric liquid crystal materials (AFLC) are given in the following.

Example of a monomesogen [1]:

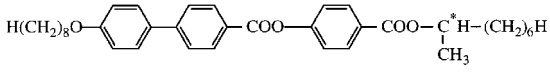

(MHPOBC)

Examples of dimesogens [7–9]:

(i) A—$(CH_2)_n$—A

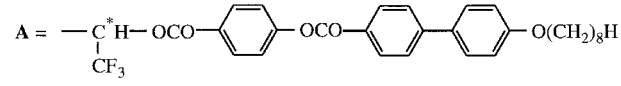

(ii)

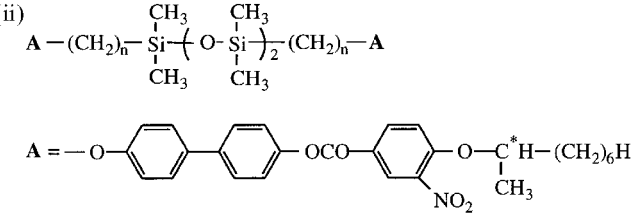

(iii) A—$(CH_2)_5$—B

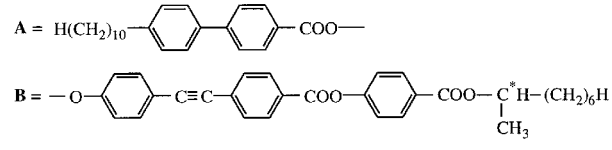

Example of a polymer [12]:

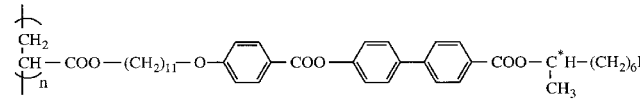

*Author for correspondence.

Address for correspondence: Institut Curie Section Physique et Chimie, 11 Rue Pierre et Marie Curie, 75231 Paris, France.

Nevertheless, no antiferroelectric *oligomer* has been reported up to now, as far as the authors are aware. Oligomers are interesting not only in the fundamental research but also in the application field. Side-attached oligomeric systems can be considered as models of side group liquid crystalline polymers, just as dimers are model compounds for main chain polymers. In the fields of information storage and optical device applications, oligomeric systems possess the advantages of both low molar mass systems and polymeric systems due to their low melt viscosities and capabilities for mesophase formation, in addition to the potential for vitrification above ambient temperature.

Here we report the synthesis and characterization of a first oligomeric antiferroelectric liquid crystal, a chiral trimesogen:

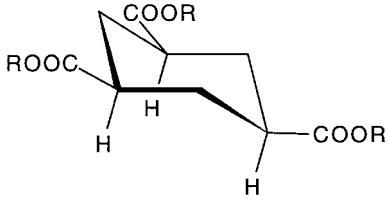

with

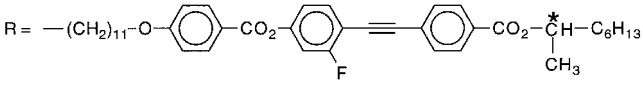

In our design of this trimesogen, three identical rod-like mesogenic moieties *R* are joined onto a cyclohexane ring in the *cis*-1-, 3- and 5-positions. The *R* group used here is susceptible to displaying the antiferroelectric phase. The choice of the cyclohexane ring maintains compatibility with the aliphatic spacer in the mesogenic moieties and generates the possibility of obtaining glass-forming liquid crystals due to its excluded-volume effect [13].

What is most interesting is that the TGBA phase and some interesting subphases are also displayed in the phase sequence, in addition to the SmC_A^* phase:

$$I–BP–TGBA–SmC^*–SmC^*_{FI(2)}–SmC^*_{FI(1)}–M1–SmC^*_A–Cr$$

In the following sections, we will describe the synthesis of the trimesogen and the corresponding monomesogens (§2) and their mesomorphic properties (§3). Structural analyses by X-ray scattering, helical pitch measurements and electro-optical studies of the trimesogen will be described in §4, §5 and §6, respectively.

2. Synthesis

The mesogenic procursor, the trimesogen and the corresponding monomesogens were prepared according to the following schemes. Details of the synthesis are reported in §8.

2.1. *Synthesis of the mesogenic procursor*

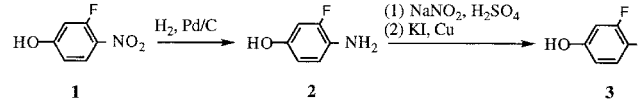

1 2 3

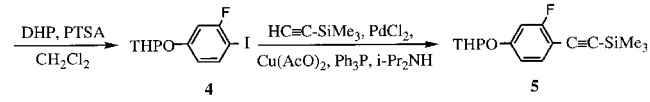

4 5

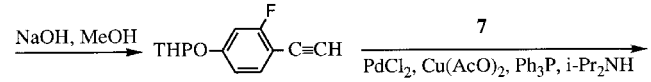

6

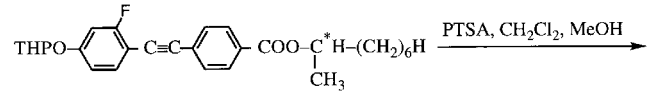

8

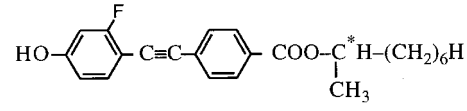

9

where the compound 7 is

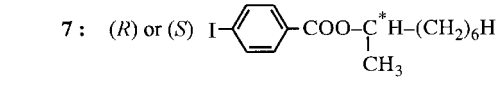

the synthesis of which has been described in ref. [14].

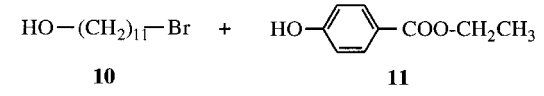

10 11

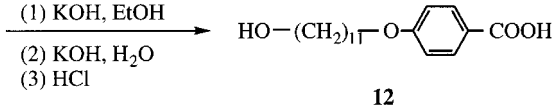

12

$$9 + 12 \xrightarrow[CH_2Cl_2]{\text{DCC, DMAP}}$$

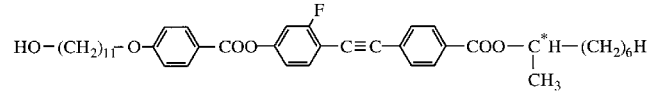

13

2.2. *Synthesis of the trimesogen*

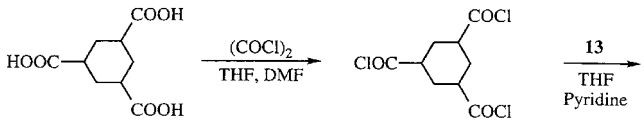

14 15

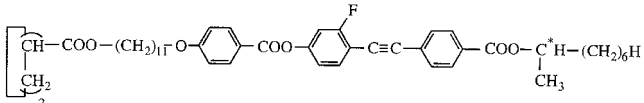

16

denoted as (*R*) or (*S*)-Cycle11(HF)

2.3. *Synthesis of the monomesogens*

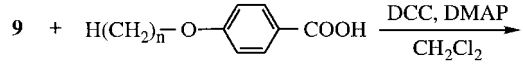

17

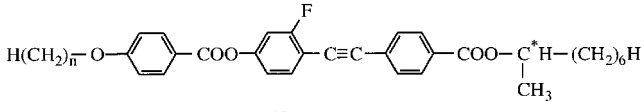

18

denoted as (*R*)-HH/HF/HH-*n*BTMHC
terminal chain length $n = 9, 10, 11, 12, 13, 14, 15, 18$

3. Mesomorphic properties

The mesomorphic properties of the monomesogens and the trimesogen obtained were studied by polarized light microscopy and differential scanning calorimetry. We used a Leitz Ortholux microscope equipped with a Mettler FP5 hot stage for optical observation and a Perkin-Elmer DSC7 for the calorimetric study.

The phase behaviour of the monomers (*R*)-HH/HF/HH-*n*BTMHC with different terminal chain length *n* is summarized in table 1. When $n \leqslant 11$, only SmA phases are displayed by the compounds. When $n = 12 \rightarrow 15$, the ferrielectric phase SmC^*_{FI} and the ferroelectric phase SmC* were observed, as well as the SmA phase. The appearance of the SmC^*_{FI} phase was marked by the typical whitish fluctuating texture in the homeotropic alignment. The SmC^*_{α} phase was only detected by DSC for $n = 14$ and 15, a shoulder peak being visible on the peak for the transition SmC*–SmA. For the derivative with the longest chain ($n = 18$), the SmC^*_{FI} disappears and the SmC* and SmA phases remain.

In most antiferroelectric compounds, the ferrielectric phases coexist with the antiferroelectric phase in the same sequence. The fact that no SmC^*_A phase was observed below the SmC^*_{FI} in the cases where $n = 12 \rightarrow 15$ is probably because the transition temperature of $SmC^*_{FI} \rightarrow SmC^*_A$ is too low and it would lie below the recrystallization temperature. Therefore, we considered that the monomers with $n = 12, 13, 14, 15$ are potentially antiferroelectric. This was the reason for the choice of the precursor with the aliphatic spacer $n = 11$ for the synthesis of the trimer. The virtual chain length per mesogen in the trimer is, in this way, between 14 and 15 when the ester group and the cycle part are included.

The phase behaviour of the trimer (*R*)-Cycle11(HF) is summarized in table 2 and the DSC thermograms are depicted in figure 1. We discuss now the assignment of the different phases displayed by the trimer.

3.1. *Fog phase (BPIII)*

Upon cooling from the isotropic phase, no detectable texture was observed microscopically in spite of the evidence for a phase given by the broad C_P variation in the DSC thermogram. We suppose this is a fog phase (BPIII), the local molecular structure of which will be discussed in the § 4.

3.2. *TGBA phase*

Further cooling results in the appearance of colourful filaments and then coloured textures invade all the sample. This is the TGBA phase confirmed by the following observations.

(1) With planar alignment, Grandjean textures with selective reflectance colours were observed in this phase (see § 5 for the helical pitch measurement).
(2) The contact preparation between the (*R*) and (*S*) enantiomers of the trimer showed in the racemic region focal-conic and homeotropic textures of a SmA phase just below the isotropic phase. We will discuss the structure of the TGBA phase in § 4.

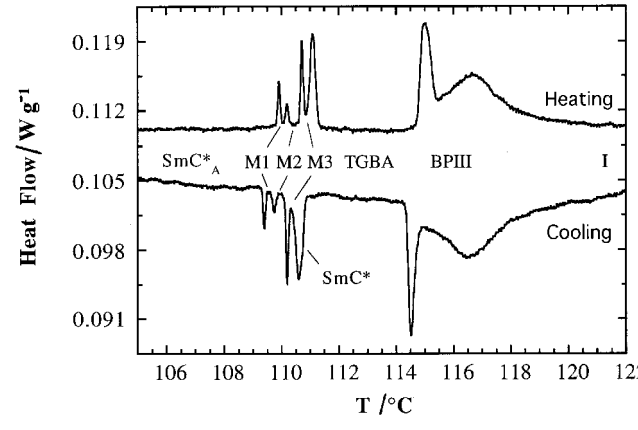

Figure 1. DSC thermograms for (*R*)-Cycle11(HF) on heating and on cooling at 0·2°C min^{-1}. The domain of the SmC^*_A phase is very large—about 47°C upon heating and about 54°C upon cooling. According to the textures, M1 corresponds to the SmC* phase and M2 and M3 correspond, respectively, to the $SmC^*_{FI(1)}$ and $SmC^*_{FI(2)}$ phases.

Table 1. Transition temperatures[a] (°C) and enthalpies (in brackets) (KJ mol^{-1}) for the monomesogens (*R*)-HH/HF/HH-*n*BTMHC ($n = 9 \rightarrow 15, 18$); temperature rate 2°C min^{-1}.

n	Mode	Cr		$SmC^*_{FI(1)}$ [b]		$SmC^*_{FI(2)}$ [b]		SmC*		SmC^*_α		SmA		I
9	Heating	•	69·8 (24·44)	—		—		—		—		•	120·1 (5·07)	•
10	Heating	•	65·1 (26·81)	—		—		—		—		•	119·6 (5·32)	•
11	Heating	•	68·1 (40·74)	—		—		—		—		•	116·4 (4·96)	•
12	Heating	•	50·6 (36·54)	•	74·6[c]	—		•	85·5 (0·026)	—		•	113·8 (5·02)	•
	Cooling	•	38·6	•	73·4[c]	—		•	84·8 (0·043)	—		•	112·3 (4·80)	•
13	Heating	•	61·4 (43·08)	•	82·5[c]	—		•	92·5 (0·086)	—		•	111·6 (4·76)	•
	Cooling	•	50·0 (42·44)	•	79·0 (0·007)	•	84·8 (0·007)	•	91·7 (0·104)	—		•	110·2 (4·63)	•
14	Heating	•	66·3 (49·86)	•	78·4 (0·012)	—		•	93·9	•	95·4 (0·198)[d]	•	110·0 (4·69)	•
	Cooling	•	55·3 (48·22)	•	74·5 (0·012)	—		•	92·5	•	94·6 (0·156)[d]	•	108·7 (4·49)	•
15	Heating	•	60·0 (47·30)	•	72·6[c]	—		•	96·0	•	96·9 (0·251)[d]	•	108·0 (4·53)	•
	Cooling	•	47·2 (42·92)	•	69·2[c]	—		•	94·9	•	96·1 (0·230)[d]	•	106·6 (4·29)	•
18	Heating	•	62·3 (53·43)	—		—		•	96·5 (0·243)	—		•	103·7 (4·68)	•
	Cooling	•	43·5 (49·65)	—		—		•	95·6 (0·230)	—		•	102·4 (3·92)	•

[a] Peak temperatures in DSC thermograms were taken as transition temperatures.
[b] $SmC^*_{FI(1)}$ and $SmC^*_{FI(2)}$ phases were distinguished in the case of $n = 13$ only by the existence of two small peaks in the DSC thermogram on cooling for the transitions SmC* → $SmC^*_{FI(2)}$ and $SmC^*_{FI(2)} \rightarrow SmC^*_{FI(1)}$. Under the microscope, the difference between $SmC^*_{FI(1)}$ and $SmC^*_{FI(2)}$ phases was not observable. When there was only one detectable ferrielectric phase, it was assigned as $SmC^*_{FI(1)}$ without structural verification.
[c] Transitions observed only under the microscope.
[d] Sum of transitions SmC*–SmC^*_α and SmC^*_α–SmA.

Table 2. Transition temperatures[a] (°C) and enthalpies (in brackets) (KJ mol^{-1}) for the trimesogen (*R*)-Cycle11(HF); temperature rate of DSC is 0·2°C min^{-1}.

Mode	Cr		SmC^*_A		M1		$SmC^*_{FI(1)}$		$SmC^*_{FI(2)}$		SmC*		TGBA		BP		I
Heating	•	62·3[b] (40·7)	•	109·9 (0·31)	•	110·2 (0·19)	•	110·7 (0·73)	•	111·1 (1·50)	—		•	115·0 (3·23)	•	116·6 (7·09)	•
Cooling	•	37·5[b] (34·8)	•	109·4 (0·27)	•	109·7 (0·23)	•	110·2 (0·72)	•	110·6 (1·66)[c]	•	110·7	•	114·5 (2·54)	•	116·5 (7·52)	•

[a] Peak temperatures in DSC thermograms were taken as transition temperatures.
[b] The data were obtained in scans at 2°C min^{-1}. The melting peak is rather sharp with width $\Delta T = 2{\cdot}5$°C; the recrystallization peak is much broader with $\Delta T \approx 33$°C, indicating very slow dynamics of recrystallization.
[c] The sum of the enthalpies of the transitions $TGB_A \rightarrow$ SmC* and SmC* → $SmC^*_{FI(2)}$.

3.3. *SmC*, SmC^*_{FI} and M1 phases*

Without special surface treatment, the transition from the TGBA phase to the SmC* phase was marked by the disappearance of the colourful textures in favour of a pseudo-homeotropic texture in most parts of the sample. The existence range of the pseudo-homeotropic texture of the SmC* phase is very brief; it appears briefly and is soon replaced by the whitish fluctuating texture of

SmC^*_{FI} on further cooling. Upon heating, no SmC* phase was observed probably through superheating of the SmC^*_{FI} phase.

There is a sharp peak in the DSC thermograms to distinguish the two ferrielectric phases $SmC^*_{FI(1)}$ and $SmC^*_{FI(2)}$, whereas the difference between them as seen in the microscope is trivial.

When the temperature is decreased slowly ($0{\cdot}2°C\,min^{-1}$), the whitish fluctuating SmC^*_{FI} texture disappears suddenly and is replaced by a spherulitic texture (see figure 2) with two colours (rose and green) separated by crossed black brushes. Circular striations are visible in the spherulites (see also § 5). In the planar aligned part of the sample, there is a small change to a broken focal-conic texture. This spherulitic texture exists over a very brief range (about 0·3°C) and corresponds to the M1 phase indicated in the DSC thermogram. This texture is very similar to that of the ribbon phase (tilted antiphase, SmC) first observed in terminal polar substances [15] and that of a chiral tilt modulated phase (SmC*) recently proposed for some chiral non-symmetric dimesogens [16]. Therefore we think this phase M1 is a chiral tilt modulated phase (SmC*). Nevertheless, this needs to be confirmed by further structural study.

3.4. *SmC^*_A phase*

With the disappearance of the spherulitic texture upon cooling, a pseudo-homeotropic texture reappears. To investigate in detail the nature of this phase, we have carried out the following experiments.

First, the racemic mixture of (*R*) and (*S*) enantiomers of the trimer was prepared and observed under the microscope. The phase sequence of the racemic mixture is:

I 115·1 SmA 107·7 SmC 105·1 SmC_A

(upon cooling at $1°C\,min^{-1}$)

A schlieren texture with only $S = \pm 1$ defects was displayed by the SmC phase domain, whereas in the lower temperature domain $S = \pm 1/2$ defects were also observable in addition to the $S = \pm 1$ defects (see figure 3); these are characteristic of a SmC_A phase [17]. The SmC^*_{FI} and M1 phases of the enantiomers disappear in favour of the SmC phase in the racemic mixture.

Secondly, a miscibility test was made between the trimer and a known antiferroelectric material [18]:

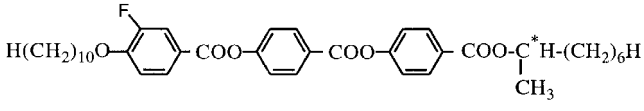

Cr 89 SmC^*_A 101·8 SmC^*_{FI} 103·4 SmC* 112·8 SmC^*_α 113·3 SmA 127 I

In the temperature domain from 101 to 90°C, the mesophase of the trimer is perfectly miscible with the SmC^*_A phase of the above standard material, proving the occurrence of a SmC^*_A phase in the trimer.

Helical pitch measurement also supports the assignment as a SmC^*_A phase (see § 5).

4. X-ray structural analyses

X-ray scattering experiments on the trimer (*R*)-Cycle11(HF) were performed in LURE (Orsay, France) using synchrotron radiation. The wavelength ($\lambda = 1{\cdot}45$ Å) was selected by a Ge monochromator. The X-ray beam at the sample position probed a $0{\cdot}5\,mm^2$ area and the scattering beam was recorded on the detector (imaging plate) situated at about 400 mm from the sample. The q domain investigated is 0·05 to $0{\cdot}25\,Å^{-1}$. The resultant instrumental resolution measured on a paraffinic powder sample (tricosane) was HWHM $\approx 1{\cdot}7 \times 10^{-3}\,Å^{-1}$ (half width at half maximum). A powder sample of the trimer was prepared in a 1-mm-diameter Lindemann capillary. The capillary was placed in a two-stage oven where the temperature could be controlled with an accuracy of 0·01°C. The calibrated temperature shift between this oven and that in the DSC technique is T_{oven}-$T_{DSC} \approx 0{\cdot}8$ to 0·9°C.

Measurements were made on cooling from isotropic liquid to SmC^*_A phase. Only one Bragg peak was observed in the q domain studied for all the phases except the biphasic domain of SmC* and TGBA, where two peaks appeared very close together. The layer spacing (d) and HWHM of the Bragg peaks as a function of temperature are depicted in figures 4 and 5, respectively.

Let us discuss first the BPIII and TGBA phases. Figure 6 shows the diffraction intensities as a function of wave vector (q) recorded during the same time (5 min) in the BPIII and TGBA phases. In BPIII near the BPIII–TGBA transition, there is already present a certain local smectic order ($d = 41{\cdot}20$ Å, HWHM $= 3{\cdot}3 \times 10^{-3}\,Å^{-1}$). This phenomenon has already been observed in another series of compounds, (*R*)-FH/FH/HH-*n*BTMHC, and discussed in detail [14, 19, 20]. It seems that the BPIII is different from the ordinary blue phase observed in the sequence N*–BP–I in its local structure. In the TGBA phase, the diffraction peak becomes stronger and sharper (HWHM $= 2{\cdot}4 \times 10^{-3}\,Å^{-1}$); the correlation length of the smectic order also increases. The asymmetry is obvious in the diffraction profiles which are reinforced on the high q side of the peaks. This can be explained by the anisotropy of the correlation lengths in the direction parallel to the layer planes and in the perpendicular direction, associated with a twist grain boundary structure [21–23].

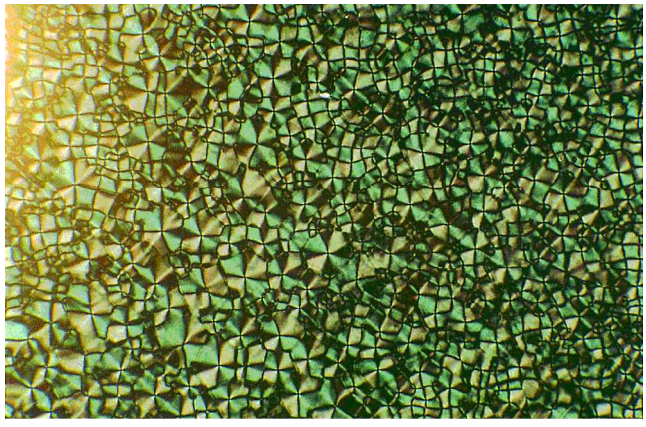

Figure 2. Spherulitic texture of the M1 phase observed at 107·9°C. Circular striations are visible in the spherulites.

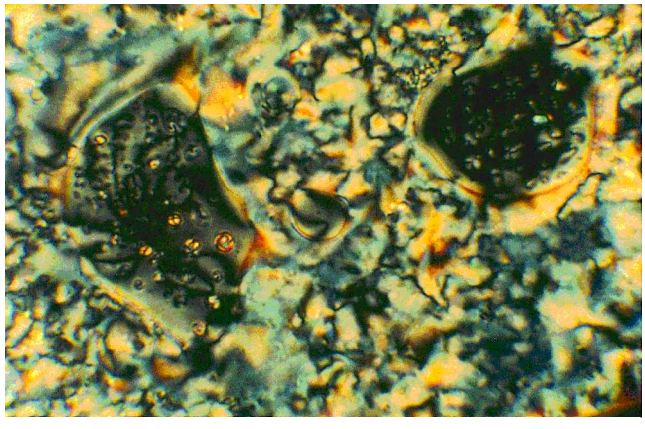

Figure 3. Texture of the SmC_A phase at 101·7°C for the racemic mixture of (*R*) and (*S*)-Cycle11(HF). The $s = \pm 1/2$ defects are visible in addition to the $s = \pm 1$ defects.

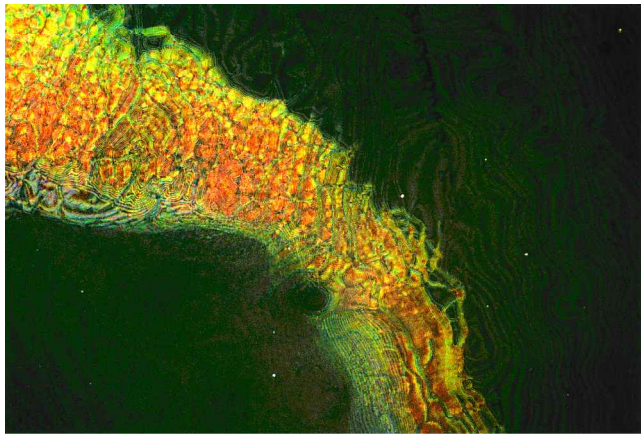

Figure 10. Textures observed using a flat pseudo-homeotropic drop at 109·6°C. From left bottom to top right, we distinguish the SmC_A^*, SmC* (striated and orange coloured) and SmC_{FI}^* phases.

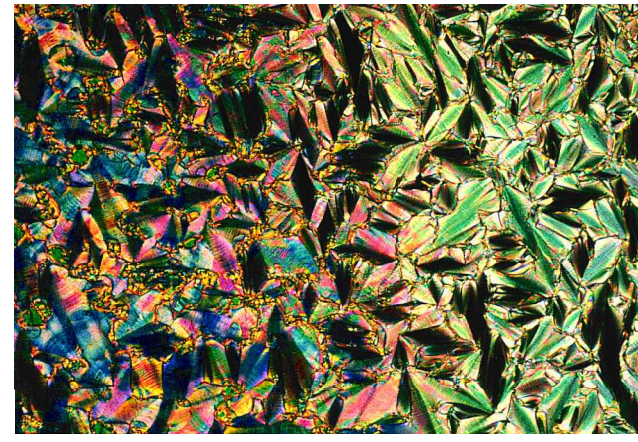

(*a*)

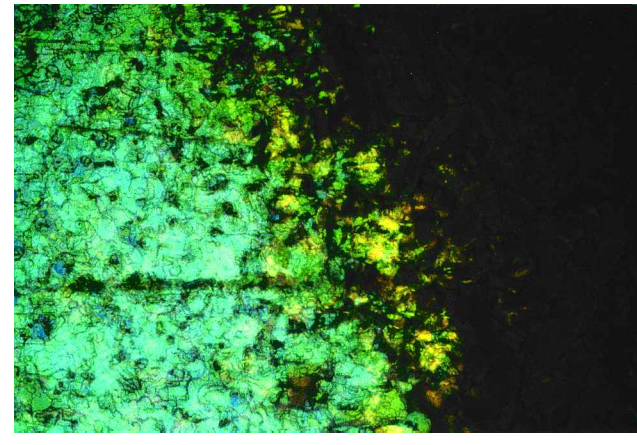

(*b*)

Figure 11. Textures observed at 110·2°C with transmitted light (*a*) and reflected light (*b*) in a low angle prismatic cell with planar orientation. In (*a*) striated focal-conics characteristic of the ferrielectric phase are seen; on the left side, we distinguish unusual colours. In (*b*) selective reflection colours of the TGBC phase are visible on the left side.

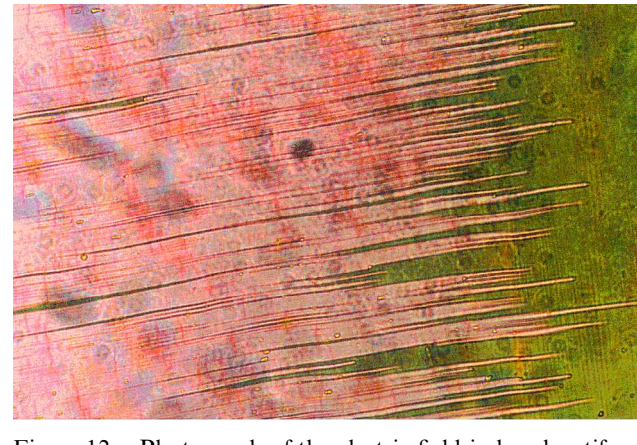

Figure 12. Photograph of the electric field induced antiferro-→ferro-electric phase transition at 100°C under a square voltage wave ($V = \pm 20$ V, $\nu = 20$ Hz). The mauve part corresponds to the ferroelectric phase and the dark green part to the antiferroelectric phase.

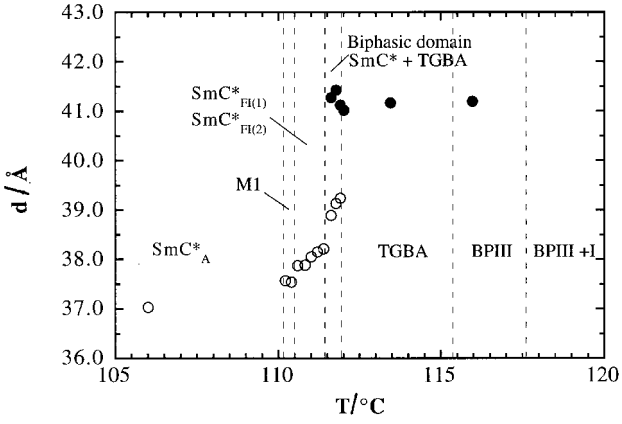

Figure 4. Layer spacing (d) versus temperature (T) in the different phases. Dotted lines separate the different phases.

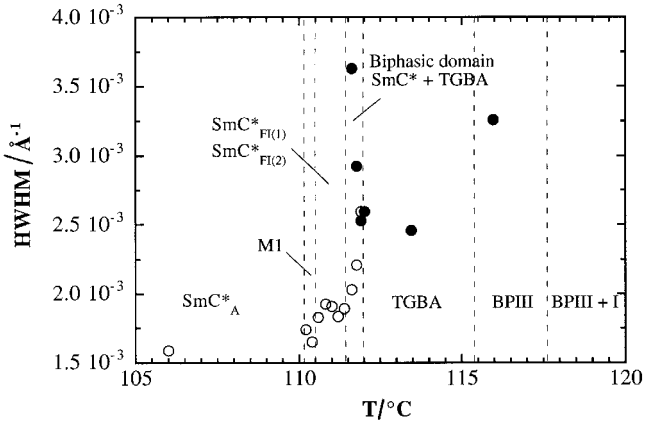

Figure 5. Half width at half maximum (HWHM) of the Bragg peak versus temperature. Dotted lines separate the different phases.

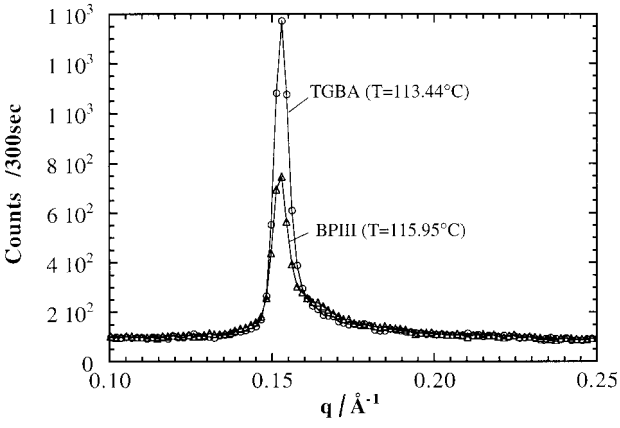

Figure 6. Comparison of the X-ray scattering intensity profiles in the BPIII and TGBA phases recorded during the same time.

On approaching the SmC* phase, there is a SmC* and TGBA biphasic domain of about 0·5°C where two Bragg peaks are recorded: d(TGBA) = 41·13 → 41·28 Å and d(SmC*) = 39·24 → 38·90 Å. The TGBA peak becomes weaker and broader on cooling (HWHM = $2{\cdot}5 \times 10^{-3} \rightarrow 3{\cdot}6 \times 10^{-3}$ Å^{-1}) and then disappears, whereas the SmC* signal becomes stronger and sharper (HWHM = $2{\cdot}6 \times 10^{-3} \rightarrow 2{\cdot}0 \times 10^{-3}$ Å^{-1}). But, there is no monophasic domain for the SmC* phase, as observed in the DSC thermogram (figure 1). The SmC^*_{FI} phases are formed directly (d = 38·21 → 37·88 Å).

In the SmC^*_A phase, the layer spacing decreases slowly with decreasing temperature, d = 37·04 Å at 106°C. The Bragg peak is rather sharp and becomes resolution limited at low temperatures.

We will try to discuss now the molecular models in the different phases. From the point of view of steric interaction and dense packing, it is more plausible that the trimer adopts a tuning-fork-like shape in bulk [24] [figure 7 (*a*)]. The layer spacing d in the SmA structure

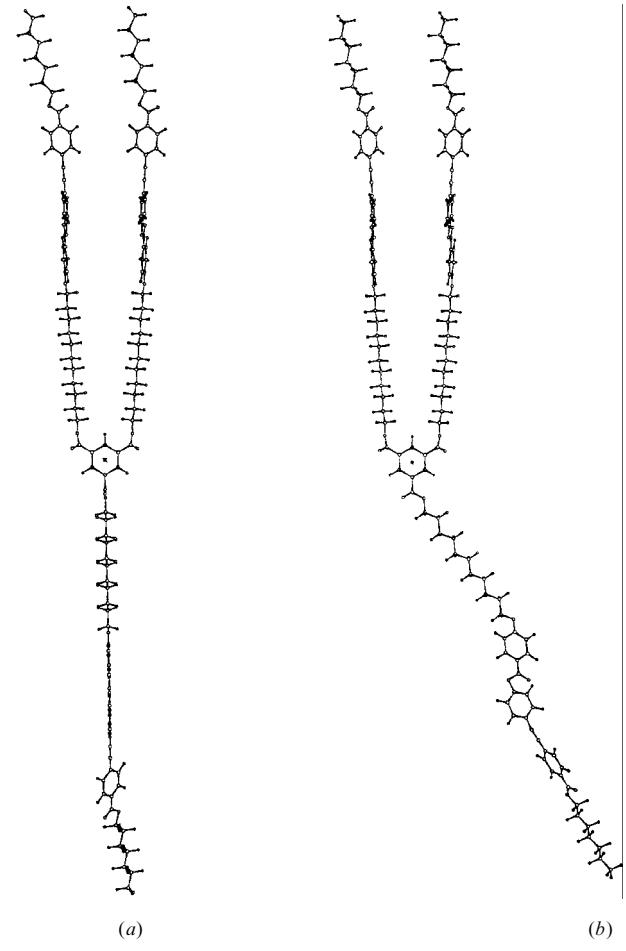

Figure 7. (*a*) and (*b*). Possible conformations of the trimesogen molecule in the isolated state; obtained by modellization with MM2* (PRCG).

of the TGBA phase is ~41 Å. This value corresponds to the average length of the single calamitic moieties attached to the ring (their extended length $l = 44$ Å) and does not correspond to the total length of the molecule in the tuning-fork-like conformation ($L = 88$ Å). A packing model shown in figure 8 (*a*) can be proposed for the molecular arrangement [24], where the layer period is $d = 1/2L$.

In the SmC* phase, the layer spacing d is about 39 Å [$d = 1/2(L \cos\beta)$ with $\beta = 28°$]. A packing model is proposed in figure 8 (*b*). The layer spacing in the SmC_A^* phase is smaller ($d = 37{\cdot}5 \rightarrow 37{\cdot}0$ Å) and corresponds to half the total length of the tuning-fork like trimer [$d = 1/2(L \cos\beta)$ with $\beta = 32 \rightarrow 33°$]. The bend of the tuning-fork [see figure 7 (*b*) for an example] seems to be necessary for the molecules in SmC_A^* phase where the calamitic moieties tilt in the opposite sense in adjacent layers. Nevertheless, the helical structures raise an important question: how do the molecules precess on a cone of revolution around the layer normal from layer to layer in the SmC* and SmC_A^* phases? Do the calamitic moieties precess separately or does the molecule in its tuning-fork-like shape precess in its entirety?

From the similarity of the texture, we have proposed that M1 is a tilt modulated phase (SmC̃*), where an undulation of the smectic layers perpendicular to the layer normal exists. The period of undulation should be characterizable by X-ray investigation. In our X-ray experiments on powder samples, we have observed unfortunately only one Bragg peak; this is probably because of the limited q domain (0·05 to 0·25 $Å^{-1}$). A larger q domain, especially in the smaller angle region, should be used, and an oriented sample is more appropriate in order to confirm the tilted antiphase structures.

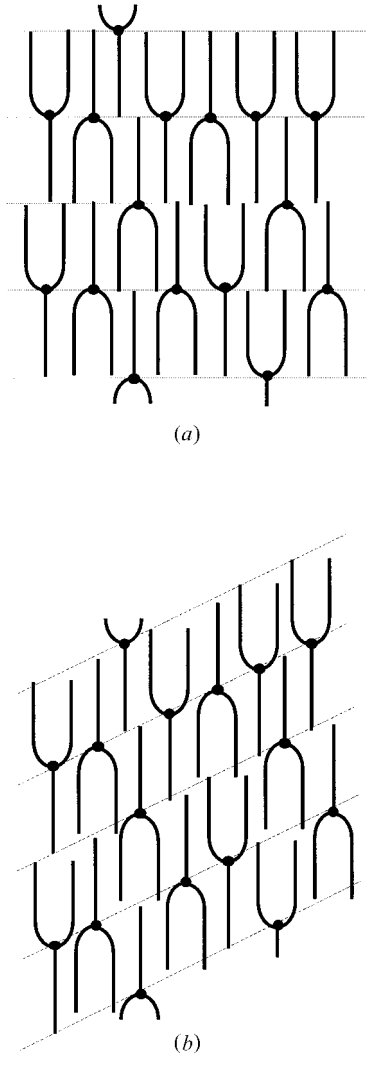

Figure 8. (*a*) Packing model for the SmA structure; (*b*) Packing model for the SmC structure.

5. Helical pitch measurements and optical observations

Helical pitch measurements on the TGBA phase were performed by the well known Grandjean–Cano method using low angle (about 0·5°) prismatic cells with a planar orientation [25, 26]. The selective reflection of light was analysed at the same time. This method is not convenient for the other phases in which a good Grandjean–Cano pseudo-homeotropic texture cannot be obtained. For this reason, measurements on the SmC* and M1 phases have been made by analysis of the light selectively reflected by pseudo-homeotropic flat drops; the visible wavelengths reflected by our compounds correspond to $\lambda = 2np$ for the SmC* phase and $\lambda = np$ for the M1 phase.

The pitch in the SmC_A^* phase is very short and does not give rise to any visible reflected light, and we had to use a particular method that had previously been applied to study SmC* [27] and SmC_α^* [28] phases: this method compares Friedel fringes observed on very flat homeotropic drops, resulting from periodic ($P/2$) ellipticity variations, to wedge fringes.

The variations of the helical pitch in the different phases are given in the figure 9. The pitch of the SmC_A^* phase is very short: 0·075 μm at $T < 108$°C; after a small decrease at $T = 108{\cdot}8$°C, the pitch slowly increases up to 0·12 μm at 109·4°C; then it grows suddenly and reaches a plateau 0·43 μm in the M1 phase where the sample shows an orange selective reflection colour. The transition $SmC_A^* \rightarrow$ M1 phase is marked by a furtive crossing of the visible spectrum. In this M1 phase, the spectrum of the reflected light is wide: its width is about three times that of the spectrum $\lambda = np$ for a SmC_A^* phase observed in another compound. This fact is probably linked to a large dispersion of the helical axial direction which does not lie strictly perpendicular to the sample and it has to be considered in relation to the

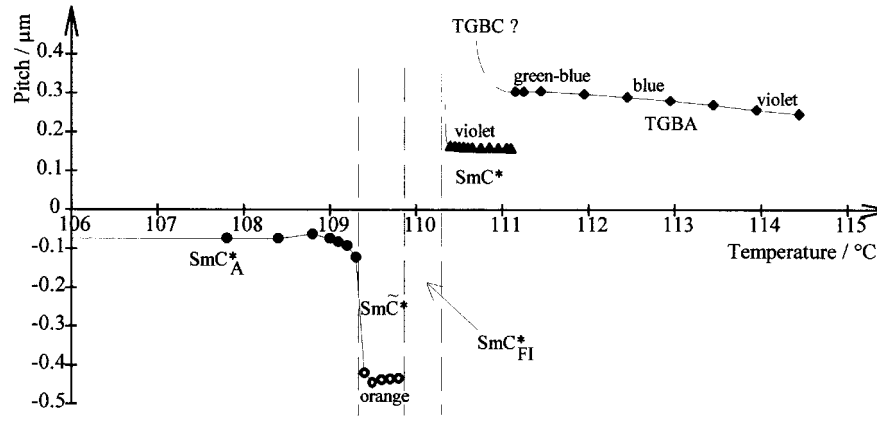

Figure 9. Helical pitch value versus temperature.

peculiar texture of this phase observed for flat drop samples (figure 10), which appears orange coloured and periodically striated. We note that if the M1 phase were confirmed to be a tilt modulated phase (SmC*), it would be the first time that a helical structure has been observed in a modulated phase.

In the ferrielectric phases, the sense of the helix changes, but we cannot give any information about the pitch values for this region.

In the SmC* phase, the pitch is short and quasi-constant: about 0·16 μm at 111°C near the TGBA phase and 0·165 μm near the ferrielectric phase, producing violet selective reflection of light with $\lambda = 2np$. The SmC*–$SmC^*_{FI(2)}$ transition is marked by a rapid increase of the pitch, visible as a furtive crossing of two visible spectra.

In the TGBA phase, the pitch lies between 0·24 μm at 114·5°C and 0·30 μm at 111·2°C, selective reflection colours varying between violet and green–blue. Additional observations showed that the compound studied has a peculiar tendency to form a TGBC phase instead of a SmC* phase.

On cooling a planar sample from the TGBA phase, the TGB texture can be maintained in some regions. They seem to be TGBC regions which differ from TGBA in their higher pitch values and green, orange and even grey colours. These regions then coexist with SmC* focal-conics regions. The TGB texture can sometimes be maintained down to the SmC^*_{FI2} phase and it transforms then into striated focal-conics characteristic of a long pitch ferrielectric smectic phase. Some of the striated focal-conics, curiously coloured when observed with transmitted light, present the same selective reflection colours as the TGBC phase, when observed with reflected light [figures 11(*a*) and 11(*b*)]. Such areas probably have a double twist structure, one helix being perpendicular to the smectic layers (in the sample plane), revealed by dechiralization lines, and the TGB helix being perpendicular to the sample plane, revealed by the selective reflection colours.

These TGBC regions can also appear at low temperature in a homeotropic sample. At high temperature, the TGBA phase is completely wound up and shows in this geometry cholesteric like focal-conics, due to the orientation of the helical axes in the sample plane. At lower temperature, the SmC* phase generally appears in two different textures: the pseudo-homeotropic texture, with violet selective reflection colours, containing numerous filaments characteristic of the TGB phase; and the focal-conic texture in which the TGBC regions are totally wound up. Some filaments can be maintained down to the ferrielectric phase.

Finally, we note that the TGBC structure has not been observed by X-ray scattering on a bulk sample and there is no signature of a TGBC phase in the DSC thermogram either. Additionally, the SmC* appears in a rather narrow domain in these two experiments. Therefore, the observation of these TGBC regions discussed above is probably related to the very small thickness of the samples.

6. Electro-optical studies

Electro-optical properties of the trimer (*R*)-Cycle11(HF) were studied using a planar geometry and 3-μm-thick commercial cells (from E.H.C. Japan). A classical set-up [29] consisted of a Eurelco 604 wave generator, a Kohn Hite 10 W wide band amplifier and a Scientific Instruments Signal Memory Recorder. The sample cell was placed in a computer controlled hot stage (temperature accuracy 0·1 K); the hot stage was mounted in an Olympus BH2 microscope for optical observations. The SmC^*_A phase exhibited by the trimer was then studied.

A simple cooling process from the isotropic phase gives a good alignment of the TGBA phase, and the uniform colour is evidence of lack of thickness variation

in the sample. The phase transition to the smectic phases, even at a very low cooling rate, induces a 'disalignment' of the sample, a typical focal-conic texture then appearing. After several unsuccessful attempts, we were able to obtain a good quality alignment in the SmC_A^* phase by applying a high electric field just below the TGBA phase transition. During the alignment process, the field value, the wave form (square or triangular) and especially the frequency are crucial. Indeed, a perfect alignment could be obtained with a square wave (± 30 V) in a frequency range of about 30–100 Hz. Nevertheless, the same signal at a frequency of 1·6 KHz completely destroyed the alignment and gave rise to a mosaic pattern of focal-conics.

The polarization measurements were made upon heating between 90 and 110°C. We were not able to make measurements below 90°C in the SmC_A^* phase because of the very high field value required to induce the antiferro- →ferro-electric phase transition (± 75 V at 90°C). Figure 12 shows the electric field induced antiferro- →ferro-electric phase change characterized by the propagation of types of 'unwinding lines' parallel to the smectic layers [30]. The mauve colour corresponds to the ferroelectric structure and the dark green colour to the antiferroelectric structure. The field value necessary to induce the antiferro- →ferro-electric phase transition is the 'threshold field' [31, 32] and the strong threshold field is one of the electro-optical characteristics of the antiferroelectric phase [33]. The threshold field increases dramatically with decreasing temperature. Thus the polarization measurements were made using a square voltage wave of between ± 25 V at 109°C and ± 75 V at 90°C, at a frequency of 20 Hz. For such field values, the saturation plateau of polarization is reached for each temperature. The values of the polarization are quite high (see figure 13). They vary from 40 nC cm^{-2} at 109°C to 62 nC cm^{-2} at 90°C.

The electrical response time (corresponding to the maximum of the polarization peak) is about 116 μm at 90°C under a square voltage wave of ± 75 V. The apparent tilt angle measurements were made with the same field as for the polarization measurements, but at very low frequency (0·2 Hz). The values are between 31·5° at 90°C and 19° at 110°C (see figure 14). Measurement was stopped at 110°C, the high temperature limit of the SmC_A^* phase in a bulk sample. Nevertheless, the field induces a TGBA → ferro-electric phase transition [34, 14] and it is possible to measure the polarization and tilt angle a few degrees into the TGBA phase.

7. Discussion and conclusions

We report here a new antiferroelectric liquid crystal material: a cyclohexane based trimesogen with a very large domain of SmC_A^* phase, extending from 109 to 54°C upon cooling. In our design of the trimer, we used a mesogenic moiety with latent SmC_A^* characteristics, but not showing AFLC properties in its monomer form. The cyclohexane core therefore plays an important role in the appearance of the SmC_A^* phase. Due to the excluded-volume effect of the cyclohexane ring, we can expect to obtain a glass-forming AFLC on modifying the ring substitution mode—for example, using the axial-equatorial *trans*-mode in place of the all-equatorial *cis*-mode [35]. Other volume-excluding central cores such as all-*exo*-bicyclo[2,2,2]oct-7-ene and cubane [36] could also be used to try to obtain glass-forming oligomeric AFLC.

The SmC_A^* phase of the trimesogen possesses very short pitch values (~0·075 μm) and the sense of the helix is opposite to that in SmC* phase at higher temperatures. Rather high spontaneous polarization values are exhibited by the SmC_A^* phase (62 nC cm^{-2} at 90°C with a response time of 116 μs and an apparent tilt angle of 31·5°).

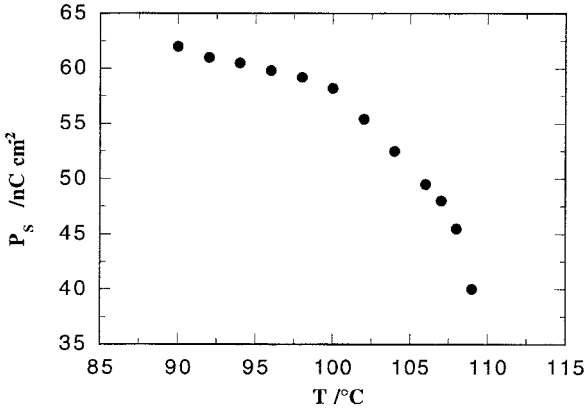

Figure 13. Spontaneous polarization versus temperature (V varying from ± 75 V at 90°C to ± 25 V at 109°C, $\nu = 20$ Hz).

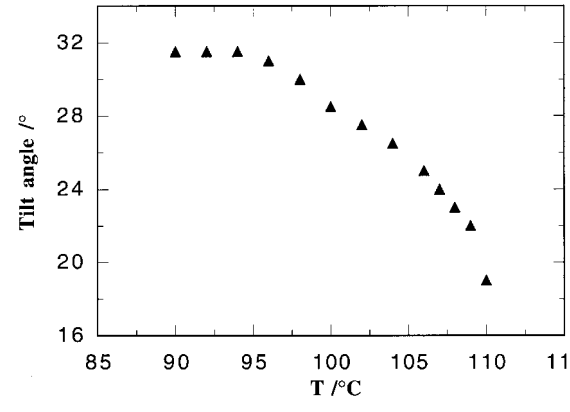

Figure 14. Apparent tilt angle versus temperature (V varying from ± 75 V at 90°C to ± 25 V at 109°C; $\nu = 0{\cdot}2$ Hz).

In addition to the SmC_A^* phase, the trimesogen displays a very rich polymorphism:

I 116·5°C BP 114·5°C TGBA 110·7°C SmC* 110·6°C

$SmC_{FI(2)}^*$ 110·2°C $SmC_{FI(1)}^*$ 109·7°C M1 109·4°C

SmC_A^* 54°C Cr.

An interesting subphase M1 was observed above SmC_A^* phase. We propose that it is a chiral tilt-modulated phase (SmC*) based on its texture. A helical structure ($P \approx 0{\cdot}43\,\mu m$) was measured in this phase. Nevertheless, the tilt-modulated structure needs to be verified by further structural studies.

8. Experimental

NMR spectra were recorded on a Bruker HW200MHz spectrometer and elemental analyses were performed by the Central Service of Analysis of CNRS.

8.1. *3-Fluoro-4-aminophenol* (2)

3-Fluoro-4-nitrophenol (10 g, 0·064 mol) was dissolved in 95% ethanol (200 ml) and 0·5 g of 10% Pt/C was added. Then hydrogen was introduced under a slight pressure. When hydrogen consumption stopped (after about 1 h), the catalyst was filtered off and the solvent evaporated. The grey powder (**2**) obtained was used immediately for the next reaction. Yield: 7·67 g (95%).

8.2. *3-Fluoro-4-iodophenol* (3)

Compound **2** (7·67 g, 0·061 mol) was dissolved in a mixture of concentrated sulphuric acid (7·3 g, 4 ml), water (30 ml) and crushed ice (30 g). The solution was cooled in a freezing bath. Under stirring, a solution of sodium nitrite (4·2 g, 0·061 mol) in 10 ml of water was added dropwise during 30 min. The solution was stirred for a further 10 min and then concentrated sulphuric acid (2·3 g, 1·2 ml) was added. The cold diazonium salt solution so obtained was poured into an ice-cooled stirred solution of potassium iodide (12·2 g, 0·073 mol) in 15 ml of water. After 5 min, 0·12 g of copper bronze was added. The solution was then warmed slowly on a water bath and maintained at 75–80°C until the evolution of nitrogen ceased. After cooling to room temperature, the crude product was extracted from the reaction mixture into 3×80 ml of chloroform. The extracts were washed with dilute sodium metabisulphite and dried with sodium sulphate. After evaporation of the solvent, the residue was filtered through silica gel with toluene as eluent. The product was finally recrystallized from heptane and plate-like crystals were obtained. Yield: 5·6 g (40%). ^{1}H NMR ($CDCl_3$): 5·08 (s, 1H, HO–Ph), 6·45–6·65 (m, 2H, *ortho* to OH), 7·26–7·58 (m, 1H, *meta* to OH).

8.3. *(R) or (S)-1-Methylheptyl 2′-fluoro-4′-hydroxytolane-4-carboxylate* (9)

The procedures of synthesis of compound **9** from compound **3** via compounds **4** → **8** were the same as those reported in ref. [14] for 1-methylheptyl 3′-fluoro-4′-hydroxytolane-4-carboxylate. ^{1}H NMR ($CDCl_3$): 0·88 (t, $J = 6{\cdot}7$ Hz, 3H, CH_2–CH_3), 1·28–1·40 (m, 13H, 5 CH_2, CH–CH_3 (d, $J = 6{\cdot}3$ Hz)), 1·58–1·82 (m, 2H, CH–CH_2), 5·16 (m, $J = 6{\cdot}7$ Hz, 1H, CH–CH_3), 6·24 (s broad, 1H, HO–Ph), 6·66 (m, 2H, arom. *ortho* to COO), 7·40 (t, 1H, arom. *meta* to OH), 7·58 (d, $J = 8{\cdot}4$ Hz, 2H, arom. *meta* to COO), 8·02 (d, $J = 8{\cdot}4$ Hz, 2H, arom. *ortho* to OH).

8.4. *4-(11-Hydroxyundecyloxy)benzoic acid* (12)

In a solution of potassium hydroxide (2 g, 0·035 mol) in ethanol (35 ml), ethyl 4-hydroxybenzoate (3·97 g, 0·024 mol) was dissolved and 11-bromo-1-undecanol (6 g, 0·024 mol) was added dropwise. The stirred solution was heated to reflux for 4 h and then cooled to room temperature. A solution of potassium hydroxide (3·38 g, 0·06 mol) in water (6 ml) was added, and the solution was reheated to reflux for 2 h. Ethanol in the solution was then removed under vacuum. The residue was dissolved in water and hydrolysed by hydrochloric acid with some added crushed ice on stirring for 1 h. The solid was filtered off and washed with water. The water remaining in the white solid was removed by adding toluene and evaporating the azeotropic mixture of water/toluene. The residue was recrystallized from absolute ethanol (white powder). Yield: 4·65 g (63%). ^{1}H NMR (CD_3COCD_3): 1·5–1·7 (m, 16H, $8CH_2$), 1·95 (m, 2H, CH_2–CH_2–Oϕ), 3·3 (broad hump, OH, COOH), 4·23 (t, 2H, CH_2–Oϕ), 7·12–7·20 (m, 2H, arom. *ortho* to OCH_2), 8·09–8·16 (m, 2H, arom *ortho* to COOH).

8.5. *(R) or (S)-1-Methylheptyl 2′-fluoro-4′-(4-(11-hydroxyundecyloxy)benzoyloxy)tolane-4-carboxylate* (13)

To a solution of phenol **9** (1·14 g, 3·10 mmol) in CH_2Cl_2 (20 ml) was added dicyclohexylcarbodiimide (DCC) (0·65 g, 3·53 mmol), 4-dimethylaminopyridine (DMAP) (0·05 g, 0·41 mmol) and 4-(11-hydroxyundecyloxy)benzoic acid, **12**, (1 g, 3·26 mmol). The resulting mixture was stirred at room temperature overnight. The solution was filtered and the solvent evaporated. The residue was purified by chromatography on silica gel with toluene as eluent. The compound (white powder) was recrystallized from heptane/ethyl acetate (20/5). Yield: 1·6 g (80%). ^{1}H NMR ($CDCl_3$): 0·88 (t, 3H, CH_2–CH_3), 1·2–1·9 (m, 31H, aliph.), 3·65 (t, 2H, CH_2–OH), 4·05 (t, 2H, CH_2–Oϕ), 5·16 (m, 1H, COO–CH–CH_3), 6·95–8·26 (m, 11H, arom.).

8.6. *Tri-4-(2-fluoro-4′-(1-methylheptyloxycarbonyl) tolane-4-oxycarbonyl) phenoxyundecyl cis-1,3,5-cyclohexanetricarboxylate* **(16)**

To a solution containing 1,3,5-cyclohexanetricarboxylic acid (0·07 g, 0·324 mmol) and a few drops of *N*,*N*-dimethylformamide in 5 ml of anhydrous THF under nitrogen was added dropwise oxalyl chloride (0·36 g, 2·86 mmol) at room temperature. After 1 h of stirring, the reaction mixture was heated to reflux for 15 min. The solvent was then evaporated off and excess of oxalyl chloride was removed under vacuum. The resultant acid chloride was dissolved in 5 ml of anhydrous THF and the solution was added to a mixture of compound **13** (0·766 g, 1·17 mmol) and pyridine (0·1 ml, 1·2 mmol) in 5 ml of anhydrous THF under nitrogen. The reaction mixture was stirred overnight before the solvent was evaporated. The solid residue was purified twice by chromatography on silica gel, using as eluent acetone/CH_2Cl_2 (1/15) for the first chromatogram and acetone/CH_2Cl_2 (1/50) for the second. The purity of the final product was controlled by HPLC. Yield: 0·29 g (40%). ^{1}H NMR ($CDCl_3$): 0·88 (t, 9H, 3 CH_2–$\underline{CH_3}$), 1·2–1·9 (m, 96H, 3 × 14 $\underline{CH_2}$, 3 CH–$\underline{CH_3}$, 3H axial in positions 2,4,6 of cyclohexane), 2·2–2·4 (m, $J = 12$ Hz, 6H, 3H equatorial in positions 2,4,6 and 3H axial in positions 1,3,5 of cyclohexane), 4·01–4·11 (m, 12H, 3 $\underline{CH_2}$–OOC, 3 $\underline{CH_2}$–Oϕ), 5·08–5·24 (m, 3H, 3 $\underline{CH}$–CH_3), 6·95–8·14 (m, 33H, arom.). Elemental analysis: C 73·63, H 7·31, F 2·63 (calculated: C74·16, H7·44, F 2·67).

8.7. *(R)-1-Methylheptyl 2′-fluoro-4′-(4-tetradecyloxybenzoyloxy) tolane-4-carboxylate* **(18)**

To a solution of phenol **9** (0·192 g, 0·52 mmol) in CH_2Cl_2 (5 ml) was added DCC (0·101 g, 0·55 mmol), DMAP (0·010 g) and 4-tetradecyloxybenzoic acid (0·184 g, 0·55 mmol). The resulting mixture was stirred at room temperature overnight. The solution was filtered and the solvent evaporated. The residue was purified by chromatography on silica gel with toluene as eluent, and was recrystallized from absolute ethanol. Yield: 0·24 g, (67%). ^{1}H NMR ($CDCl_3$): 0·89 (t, 6H, 2$\underline{CH_3}$), 1·27–1·85 (m, 37H, aliph.: 15$\underline{CH_2}$; $\underline{CH_3}$–CH (1·31, d); OCH$\underline{CH_2}$, O$CH_2\underline{CH_2}$ (1·8, m)), 4·05 (t, 2H, O$\underline{CH_2}$), 5·16 (m, 1H, $\underline{CH}CH_3$), 6·97–8·14 (m, 11H arom.).

The authors would like to thank Annick Babeau for her performance of HPLC on the trimer samples, Michel Laguerre for his assistance in obtaining the molecular models, and the LURE team on beam line D43 for their hospitality and competence. They are also grateful to Gilles Sigaud for useful discussions. They acknowledge the Nord-Pas de Calais region and the FEDER for the funding of the spectroscopic set-up used for the helical pitch measurements.

References

[1] Chandani, A. D. L., Gorecka, E., Ouchi, Y., Takezoe, H., and Fukuda, A., 1989, *J. appl. Phys.*, **28**, L1265.
[2] Levelut, A. M., Germain, C., Keller, P., Liebert, L., and Billard, J., 1983, *J. de Phys. (Paris)*, **44**, 623; Galerne, Y., and Liebert, L., 1990, *Phys. Rev. Lett.*, **64,** 906.
[3] Goodby, J. W., Patel, J. S., and Chin, E., 1991, *J. mater. Chem.*, **2,** 197.
[4] Nguyen, H. T., Rouillon, J. C., Cluzeau, P., Sigaud, G., Destrade, C., and Isaert, N., 1994, *Liq. Cryst.*, **4,** 571.
[5] Wu, S. L., Huang, F. K., Uang, B. J., Tsai, W. J., and Liang, J. J., 1995, *Liq. Cryst.*, **18,** 715.
[6] Aoki, Y., and Nohira, H., 1995, *Liq. Cryst.*, **19,** 15.
[7] Suzuki, Y. I., Isozaki, T., Hashimoto, S., Kusumoto, T., Hiyama, T., Takanishi, Y., Takezoe, H., and Fukuda, A., 1996, *J. mater. Chem.*, **6,** 573.
[8] Poths, H., Cluzeau, P., Nguyen, H. T., Mauzac, M., and Destrade, C., 1995, *FLC95, Cambridge*, p. 81.
[9] Faye, V., Nguyen, H. T., Laux, V., and Isaert, N., 1996, *Ferroelectrics*, **179,** 9.
[10] Kuehnpand, K., and Springer, J., 1991, *Makromol. Chem. rapid. Commun.*, **12,** 381.
[11] Skarp, K., Andersson, G., Lagerwall, S. T., Kapitsa, H., Poths, H., and Zentel, R., 1991, *Ferroelectrics*, **122,** 127.
[12] Nishiyama, I., and Goodby, J. W., 1993, *J. mater. Chem.*, **3,** 169.
[13] Shi, H. Q., and Chen, S. H., 1994, *Liq. Cryst.*, **17,** 413.
[14] Li, M. H., Laux, V., Nguyen, H. T., Sigaud, G., Barois, P., and Isaert, N., 1997, *Liq. Cryst.*, **23,** 389.
[15] Hardouin, F., Nguyen, H. T., Achard, M. F., and Levelut, A. M., 1982, *J. Phys. Fr., Lett.*, **43,** 327.
[16] Faye, V., Babeau, A., Placin, F., Nguyen, H. T., Barois, P., Laux, V., and Isaert, N., 1996, *Liq. Cryst.*, **21,** 485.
[17] Takanishi, Y., Takezoe, H., Fukuda, A., Komura, H., and Watanabe, J., 1992, *J. mater. Chem.*, **2,** 71.
[18] Faye, V., Rouillon, J. C., Destrade, C., and Nguyen, H. T., 1995, *Liq. Cryst.*, **19,** 47.
[19] Pansu, B., Li, M. H., and Nguyen, H. T., 1997, *J. de Phys. (II) Fr.*, **7,** 751.
[20] Pansu, B., Li, M. H., and Nguyen, H. T. (in preparation).
[21] Renn, S. R., and Lubensky, T. C., 1988, *Phys. Rev. A*, **38,** 2132.
[22] Srajer, G., Pindak, R., Waugh, M. A., Goodby, J. W., and Patel, J. S., 1990, *Phys. Rev. Lett.*, **64,** 1545.
[23] Nguyen, H. T., Bouchta, A., Navailles, L., Barois, P., Isaert, N., Twieg, R. J., Maaroufi, A., and Destrade, C., 1992, *J. Phys. II, Fr.*, **2,** 1889.
[24] Göring, P., Pelzl, G., Diele, S., Delavier, P., Siemensmeyer, K., and Etzbach, K. H., 1995, *Liq. Cryst.*, **19,** 629.
[25] Nguyen, H. T., Twieg, R. J., Nabor, M. F., Isaert, N., and Destrade, C., 1991, *Ferroelectrics*, **121,** 187.
[26] Bouchta, A., Nguyen, H. T., Achard, M. F., Hardouin, F., Destrade, C., Twieg, R. J., Maaroufi, A., and Isaert, N., 1992, *Liq. Cryst.*, **12,** 575.
[27] Brunet, M., and Isaert, N., 1988, *Ferroelectrics*, **84,** 25.
[28] Laux, V., Isaert, N., Nguyen, H. T., Cluzeau, P., and Destrade, C., 1996, *Ferroelectrics*, **179,** 25.

[29] Dupont, L., Glogarova, M., Marcerou, J. P., Nguyen, H. T., and Destrade, C., 1991, *J. Phys. II, Fr.*, **1,** 831.
[30] Carvalho, P. S., Cluzeau, P., Destrade, C., Nguyen, H. T., and Chaves, M., 1995, *Ferroelectrics*, **178,** 195.
[31] Hamelin, P., 1991, Thesis, Université Paris-Sud, France.
[32] Takezoe, H., Lee, J., Chandani, A. D. L., Gorecka, E., Ouchi, Y., and Fukuda, A., 1991, *Ferroelectrics*, **114,** 187.
[33] Cluzeau, P., 1995, Thesis, Université de Bordeaux I, France.
[34] Destrade, C., Payan, S., Cluzeau, P., and Nguyen, H. T., 1994, *Liq. Cryst.*, **17,** 291.
[35] Shi, H. Q., and Chen, S. H., 1995, *Liq. Cryst.*, **19,** 785.
[36] Chen, S. H., Mastrangelo, J. C., Blanton, T. N., Bashir-Hashemi, A., and Marshall, K. L., 1996, *Liq. Cryst.*, **21,** 683.